Physics Open 9 (2021) 100088

Contents lists available at ScienceDirect

Physics Open

journal homepage: www.sciencedirect.com/journal/physics-open

Effect of a ferromagnetic STM cobalt tip on a single Co-phthalocyanine molecule adsorbed on a ferromagnetic substrate

A. Jaafar [a,b], I. Rungger [c], S. Sanvito [d], M. Alouani [a,*]

[a] Université de Strasbourg, Institut de Physique et de Chimie des Matériaux de Strasbourg (IPCMS), UMR 7504 UNISTRA-CNRS, 23 rue du Loess, 67034, Strasbourg, France
[b] Laboratoire de Physique de Matériaux, Lebanese University, Faculty of Sciences (I), Hadath, Beirut, Lebanon
[c] National Physical Laboratory, Teddington, TW11 0LW, United Kingdom
[d] School of Physics, AMBER and CRANN Institute, Trinity College, Dublin 2, Ireland

ARTICLE INFO

Keywords:
Electronic structure
Molecule-substrate adsorption
Tunneling magneto-resistance
Electronic transport

ABSTRACT

The effect of a ferromagnetic scanning tunneling microscope (STM) cobalt tip on the electronic, magnetic and electronic transport properties of a Co-phthalocyanine (CoPc)/Co(111) junction has been investigated in the framework of density functional theory in conjunction with Landauer transport and the non-equilibrium Green function formalism. It is shown that the spin magnetic moment of the CoPc molecule can be flipped by varying the distance between the STM tip and the CoPc molecule when passing from the tunneling regime to the contact regime. Our calculations show that such spin flip of the CoPc molecule leads to a change of the sign of the *Tunneling Magneto-Resistance* ratio (TMR). The change from the tunneling to contact regime also leads to large changes in the total and spin-polarized *I–V* characteristics.

1. Introduction

The concepts underpinning molecular electronics and spintronics, offer a very promising avenue for the further miniaturization of devices in information and communication technology. A key aspect is that organic devices must be contacted by inorganic drivers to enable communication and control from the outside. Such contact, an organic-inorganic interface, can change dramatically the properties of the molecule and determine alone the functionality of the device. Therefore, the study of the contact between molecules and inorganic semiconductors or metallic substrates, is one of the most important tasks in the emerging technology of molecular electronics [1].

In molecular spintronics, the magnetism of the electrodes used for molecular junctions plays a crucial role. In addition the deposition of an organic molecule containing a magnetic atom on a metallic substrate can lead to different interesting physical phenomena such as the Kondo effect. Indeed, for temperatures below a transition temperature, called the Kondo temperature, the localized spin of the molecule is screened by the conduction electrons of the surface, giving rise to a range of features detectable with a transport measurement [2,3]. Traditionally, metal-phthalocyanine (MPc) molecules, composed of a magnetic metal atom, M, surrounded by a ligand ring, have been used in this context. These are of potential interest for spin-dependent electronics [4,5] and optoelectronics [6,7].

Several works have been performed on MPc molecules [8–15], for instance demonstrating a controllable Kondo effect [8–10,16] and directly visualizing stationary spin states of individ-ual CoPc molecules [11]. The transport through CoPc molecule junction has also been discussed [11–14,17]. In general, it has been shown that the electronic and magnetic properties of a MPc molecule strongly depend on the type of metal ion M within the phthalocyanine ligand and the type of surface on which the molecule is adsorbed [12,18].

Several theoretical and experimental works [11,17] have been performed to study the influence of magnetic and nonmagnetic substrates on cobalt-phthalocyanine, as well as the spin transport across single molecules. At the same time, there is a fast growing interest in controlling the spin orientation of a single or few magnetic atoms in a solid state environment for future spintronics and quantum information devices [19,20]. The spin direction can be driven into either a parallel or antiparallel alignment with respect to the substrate, or even in a noncollinear alignment, depending on the sign of the exchange coupling [21].

Scanning tunneling microscopy (STM) offers the ability to study single magnetic moments and the exchange coupling between spins in a

* Corresponding author.
E-mail address: mea@unistra.fr (M. Alouani).

https://doi.org/10.1016/j.physo.2021.100088
Received 7 January 2021; Received in revised form 6 May 2021; Accepted 13 July 2021
Available online 21 July 2021

precisely characterized local environment [22,23]. Thus, a single magnetic moment can be manipulated using an STM tip and offers the possibility to control or tune the magnetic properties at the atomic scale. For example, using STM, researchers have been able to control the spin state of a single magnetic adatom by depositing it on an insulating thin film [24] or on magnetic islands [25,26]. However, little is known about the influence of the STM tip on electronic and magnetic properties of molecules deposited on magnetic surfaces [3,27–31].

In this study, we will show that the tip-surface distance strongly influences the electronic and magnetic properties as well as the behavior of the conductance of a single Cophthalocyanine deposited on a cobalt metallic surface. Our aim in this theoretical study is therefore to analyze (1) the impact of the STM-tip on the electronic and magnetic properties of a single CoPc molecule adsorbed on the Co(111) surface, and (2) the effect of the STM-tip on the transport properties of the junction, in particular when making the transition from the tunneling to the contact regime.

To this end we have employed an *ab initio* pseudopotential density functional theory (DFT) methodology to study the magnetic moment of the central atom of CoPc, the transmission coefficient of STM-tip CoPc over Co(111) substrate, as well as the current-voltage, *I–V*, characteristics as function of the distance between the STM tip and the CoPc molecule. The junction adopted in our work consists of two Co(111) electrodes: a cone of cobalt atoms, which represents the magnetic STM tip, and a CoPc molecule deposited at different positions (hcp, fcc, bridge) on a second Co(111) electrode. The Co(111) substrate is modeled by a slab of 5 layers of Co atoms and the STM tip consists of 11 atoms.

In order to manipulate the spin direction of the central atom of the CoPc molecule and the conductance across the molecular junction using a magnetic STM tip, we have adopted two configurations (see Fig. 1). In the first configuration [Fig. 1-(a)], the initial spin directions of the STM tip, central atom of CoPc and Co(111) substrate are in a parallel alignment configuration (PC), whereas, in the second configuration [Fig. 1-(b)], they are in an antiparallel alignment configuration (APC).

Our manuscript is organized as follows: in the next section we describe briefly our calculation methods. Then we present and discuss our results on the adsorption energy and the electronic and magnetic properties of CoPc/Co(111). In the following section we show the effect of the magnetic STM-tip on the electronic as well as magnetic properties and the spin-dependent electric conductance for the two magnetic configurations (PC and APC).

2. Calculation methods

Our study is based on *ab initio* pseudopotential calculations using the Siesta [32] and Smeagol [33,34] codes. In particular, our study was conducted in two stages. In the first stage, we have used Siesta to determine the effects of the structure on the electronic properties of the CoPc molecule. In the second stage, we have used the Smeagol code to investigate the electronic transport properties of the parallel and antiparallel alignment of the magnetizations of the STM tip and the molecular junction. To view the challenges in a single-molecule electron transport, the reader can benefit from the recent review article of Evers and coworkers [35].

The Siesta package [32] implements a norm-conserving pseudopotential approach [36] to the DFT Kohn-Sham problem, with either the local-density approximation (LDA) [37] or the generalized gradient (GGA) approximation of the electron-electron exchange and correlation functional [38]. The one-particle Kohn-Sham equations are solved by using a linear combination of atomic orbitals (LCAO) and conjugate gradient. In the presented calculations we have used for the exchange and correlation potential the local-density approximation (LDA) of Ceperley-Alder [39]. For magnetic systems, we have performed spin-polarized calculations in the local spin-density approximation (LSDA) including van der Waals (vdW) dispersive forces within the Grimme approximation [40]. The pseudopotentials are norm-conserving [36] and factorized in the Kleinman-Bylander form [41], including scalar-relativistic effects. The valence states are described by using a double-ζ (DZ) basis sets. For cobalt, a DZ basis was used with two different radial functions to represent the 4*s* and 3*d* orbitals. For N, C and H, a DZ basis was used with two different radial functions to represent the 2*s*, 2*p* and 1*s* (for H) orbitals. Finally for our solid systems, the integration over the two-dimensional Brillouin zone is obtained using a 4×4 **k**-point grid [42]. The electronic population is sorted for each orbital on each atomic site using the Millikan population analysis.

The Smeagol (Spin and Molecular Electronics on Atomically Generated Orbital Landscape) package is a fully spin-polarized code, which combines DFT with the non-equilibrium Green's functions (NEGF) transport method [33,34]. Smeagol uses Siesta as DFT platform exploiting the fact that the operators calculated by Siesta (density matrix and Hamilotinian) are in tight-binding-like form and can be easily interfaced to the NEGF method. The NEGF method splits up a two-terminal device into three regions, a scattering region and two semi-infinite leads (the left and right leads). A bias voltage is applied by setting the chemical potential of the left and right leads to $\mu_L = E_F + eV_b/2$ and $\mu_R = E_F - eV_b/2$, respectively, where E_F is the common Fermi level of both leads and V_b is the applied bias (e is the electron charge).

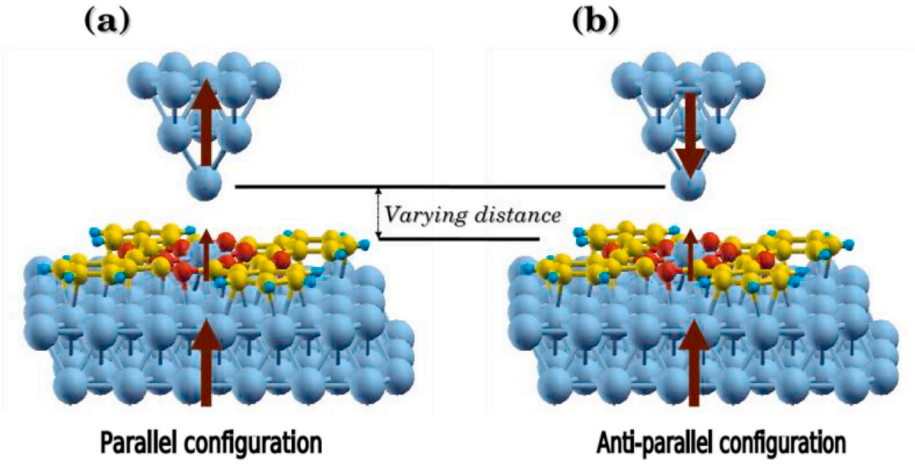

Fig. 1. STM setup: plots (a) and (b) represent, respectively, the parallel configuration (PC) and antiparallel configuration (APC) of the magnetization of the tip and the junction. The varying distance from the tip to the junction of CoPc/Cu(111) is also shown.

The current through the atomic scale system can be calculated from the corresponding Green's function and self-energies using the Landauer formula [43]:

$$I(V) = \frac{2e}{h} \int_{-\infty}^{+\infty} T(E,V)[f(E-\mu_L) - f(E-\mu_R)]dE, \quad (1)$$

where f is the Fermi distribution, h the Planck constant, and $T(E,V)$ is the transmission coefficient at energy E and bias voltage V,

$$T(E,V) = \mathrm{Tr}[\mathrm{Im}\Sigma_L(E)G^R(E)\mathrm{Im}\Sigma_R(E)G^A(E)], \quad (2)$$

where $G^{R/A}(E)$ are the retarded and advanced Green's function of the central region and $\Sigma_{L/R}$ are the coupling matrices to the left/right leads. Based on the eigenchannel decomposition of the conductance, this total transmission $T(E,V)$ can be decomposed into non-mixing eigenchannels [44–47] as follows:

$$T(E,V) = \sum_{\sigma,n} T_n^{\sigma}(E,V), \quad (3)$$

where σ is the spin index. In all our transport calculations. The complex part of the integral leading to the charge density is computed using 16 energy points on the complex semi-circle, 16 points along the line parallel to the real axis and 16 poles. The integral over real energies necessary at finite bias is evaluated at 200 points. All the calculations are carried out with periodic boundary conditions in the direction parallel to that of the transport. In addition, due to the large size of the unit cell, no k-points are used in the direction perpendicular to the transport (only the Γ point).

3. Results and discussion

3.1. Study of the CoPc/Co(111) junction

In order to investigate the interaction between the substrate and CoPc molecule, we first perform *ab initio* calculations to find the equilibrium position of the CoPc molecule adsorbed on the Co(111) surface. Several initial adsorption configurations including hollow, fcc, and bridge sites (see Fig. 2(a)) are considered to find the most stable one. The Co(111) substrate is modeled by a slab consisting of five layers. For technical considerations, we tested two periodic supercells of CoPc/Co (111): 6 × 7 and 7 × 8, with five layers of Co. For both supercells, the lattice parameter perpendicular to the surface is 30 Å, and each supercell consists, respectively, of 267 and 337 atoms, respectively, including the 57 atoms of CoPc. We have shown that the two supercells produce adsorption energies and electronic structures that are not significantly different from each other.

To obtain the Hamiltonian matrix elements, we used a real space mesh with the corresponding reciprocal space cutoff of 500 Ry and a 4 × 4 inplane k-point grid. All the geometries are optimized using the conjugate gradient until the forces on each atom are smaller than 0.02 eV/Å. The results are confirmed by PWscf *ab initio* simulation package calculations [17,18]. Note that within the strong coupling limit of the molecule with the substrate, as it is for the CoPc on Co(111), it was shown by Toher and coworkers [48] that the highest occupied molecular orbital (HOMO) and lowest unoccupied molecular orbital (LUMO) within the LDA or the GGA are very broad and the self-interaction correction to the I–V characteristics is found to be very small [48] which justifies the present use of LDA to study the transport properties of CoPc/Co(111). It was also independently shown by Neaton, Hybertsen and Louie, that the molecular electronic levels are strongly renormalized when the molecule is physisorbed on a metallic surface, i.e. the LUMO-HOMO gap called using the GW approximation is strongly reduced compared to that of the gas phase and gets closer to the DFT results [49]. This is of course less dramatic than when the molecule is chemisorbed as in our case. It is clear that the HOMO-LUMO gap present in the gas phase for CoPc, as shown by Brumboiu et al. [50], completely vanishes when the molecule is adsrobed on the Co(111) surface (see Fig. 3). The overlapping HOMO and LUMO is due to the strong hybridization of the CoPc orbitals with those of the Co(111) substrate.

Regarding the stability of the CoPc molecule on Co(111), we found that the bridge position (see Fig. 2(a)) is the most stable and the optimal distance between the molecule and the substrate is 2.049 Å. These results are in excellent agreement with previous experimental and

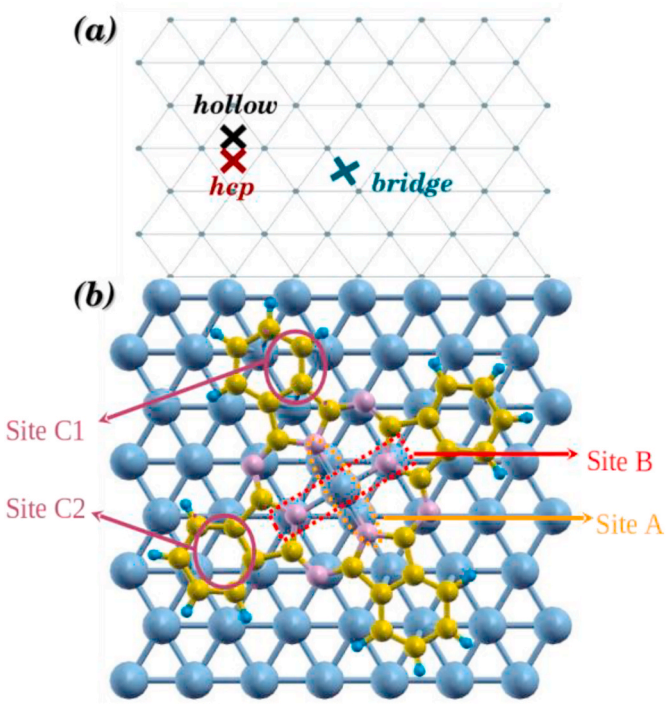

Fig. 2. (a) High-symmetry sites of Co(111) surface and (b) the position of the CoPc molecule centered on the bridge position. Each of the sites A and B represents two atoms of Co located just below the nearest four nitrogen atoms. In site A, the two Co atoms are in contact with the central atom and two N atoms, whereas the two atoms of site B are only in contact with two nitrogen atoms. Site C1 (2) represents the Co atoms forming a triangle below the benzene ring.

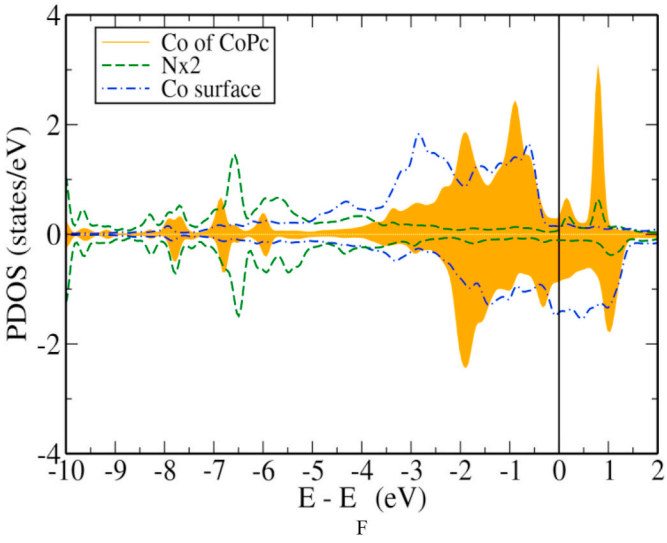

Fig. 3. Calculated spin-polarized projected density of states (PDOS) for various atoms of CoPc/Co(111). Co of CoPc (filled orange), nitrogen (green dashed curves), Co surface (blue dot-dashed curves). (For interpretation of the references to colour in this figure legend, the reader is referred to the Web version of this article.)

theoretical studies [11,17]. Our calculated relative energy and magnetic moment of the central Co atom of CoPc within the optimized structure of the CoPc molecule adsorbed on Co(111) are listed in Table 1 for each of the different adsorption sites. The difference of the relative energy between the hcp and the fcc configurations is small (80 meV), but it indicates that the fcc configuration is more stable that of hcp. In the following, we will present and discuss the results only for the most stable bridge configuration. The magnetic moment (0.34 μ_B/atom) of the central atom of CoPc molecule decreases in comparison to the free molecule value (1.1 μ_B/atom).

We also found a small negative magnetic moment for the N and C atoms of CoPc molecule. In addition, the magnetic moments of Co atoms on the surface have been modified compared to the value (1.85 μ_B/atom) of Co atoms of the free surface. For example, the magnetic moment of each Co atom on sites A and B (see Fig. 2(b)) is reduced by about 0.2 μ_B on average. In sites C1 and C2, we have an average reduction of about 0.35 μ_B and 0.32 μ_B, respectively. Indeed, these changes of the magnetic moments can be also observed from the projected density of states (PDOS). Fig. 3 represents the PDOS of the Co atom of the molecule, those of the nearest four N atoms, and the surface Co atoms. In this Figure (3), we can observe that there is a hybridization between the Co surface atoms and N atoms at binding energies between −4.7 eV and −3.8 eV. This figure shows also a hybridization between the Co atom of CoPc with the Co(111) surface in low energy range (between −5.6 and −6.3 eV, −7.5 and −8.1 eV, −9.5 and −9.7 eV). This hybridization provides the chemical bonding of the CoPc on the magnetic surface. In addition, the spin-up and spin-down PDOS of the Co in CoPc show a shift respectively to the right and to the left, which explains the reduction of the magnetic moment compared to that of the free molecule. Consequently, those modifications, that were induced on the electronic and magnetic properties of the surface's Co atoms and the atoms of the CoPc molecule, are due to a pronounced interaction between CoPc and the magnetic substrate. Here we should point out that our values are in good agreement with other results obtained by other methods [11,17].

3.2. Electronic and magnetic properties and effect of the STM tip

To explore the transport properties as a function of the distance between the STM Co-tip and the substrate in the CoPc molecular junction, i.e., from contact to tunneling regime, we have first investigated the electronic and magnetic properties of the two PC and APC configurations (see Fig. 1 (a) and (b)). We placed the STM-tip above the Co atom of the CoPc molecule, and varied the distance between the Co-tip and the CoPc from 2.05 to 6.0 Å.

Fig. 4 shows the Co magnetic moment in CoPc for both PC and APC as a function of the tip-molecule distance from the tunneling to the contact regime. Here PC indicates the parallel alignment of the tip and substrate magnetic moments, and APC an antiparallel alignment. For the PC the magnetic moment of the molecule is always aligned with the tip magnetic moment. We can observe that the value of the magnetic moment at 5–6 Å, where the interaction of tip-CoPc is weak, is very close to that found for the molecule deposited on Co(111). However, at 2.05 Å, where the interaction between the tip and CoPc is strong, the value of the magnetic moment is much larger than that obtained at 5–6 Å due to additional strong exchange interaction from the tip. As for the APC, the magnetic moments observed in the range 3–6 Å are almost the same as

Table 1
Calculated relative energy ΔE (eV) and magnetic moment μ of Co atom in CoPc for different contact geometries. The energy for the most stable position is set to zero.

	hcp	fcc	bridge
ΔE (eV)	0.90	0.82	0
$\mu(\mu_B$/atom)	0.52	0.46	0.34

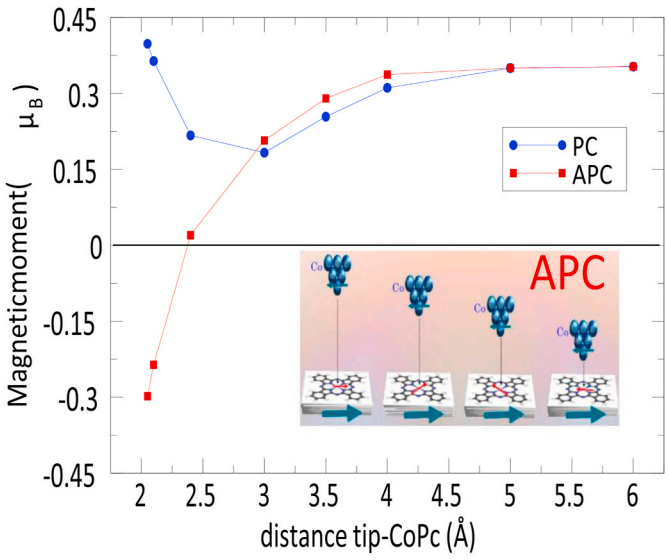

Fig. 4. Co atom magnetic moment of the CoPc molecule for the PC (parallel configuration) and APC (anti-parallel configuration) of the tip and substrate magnetic moments as a function of the tip-CoPc distance. The inset shows a schematic view of the magnetic coupling of the tip with the Co magnetic moment as the tip approaches the substrate.

those in the parallel configuration, since we are in the tunneling regime. The appealing result in the APC is the spin flip of the CoPc which starts at 2.4 Å where the magnetic moment of the central atom is almost zero. This modification of the magnetic moment depending on the distance between tip-CoPc is a well-known effect [31,51] and is attributed to the charge transfer from the tip-apex atom to the spin-down states of the ad-atom.

To explain the origin of the spin flip, we need to understand the hybridization-interaction from the electronic structures of the *s* and *d* states. For this purpose, we analyzed the electron distributions of the *s* and *d* orbitals and the density of states of the central atom. In order to make a clear comparison, we chose to present the electron distributions and the density of states at 2.05 Å (contact regime), 2.4 Å (transition regime) and 5.0 Å (tunneling regime) for both configurations. The electron distributions of *s* and *d* states are plotted in Fig. 5, and the total DOS of the central atom of CoPc is presented in Fig. 6.

This figure shows that the main contribution is obviously from the *d* states. For the *s* states, the difference between up and down charge is very small in the two configurations (PC (Fig. 5-a), and APC (Fig. 5-b)). However, it is positive in the PC and negative in APC in the contact regime where the spin flips. For the *d* states, our analysis of the electron distribution for the APC (Fig. 5-d) reveals that the tip-CoPc hybridization depletes the *spin-up d* states of the Co in CoPc, and increases the population of the *spin-down d* states which becomes the majority in the contact regime (d = 2.05 Å). We can also observe this effect by comparing the PDOS of the Co in CoPc, in the three chosen tip-CoPc distance separations, with that calculated in the CoPc/Co(111) system (see Fig. 6 (a) and (b)). The results for both spin directions are plotted where the energies are given relative to the Fermi energy. In the PC (Fig. 6(a)), both the spin-up and spin-down states show the same negative shift. It can be easily observed that the shift of the two spin states are affected by the tipsubstrate distance. However, these shifts increase when the tip-CoPc distance decreases, i.e., the interaction becomes stronger. At d = 5.0 Å, where the interaction of the tip with the Co atom in CoPc is rather weak, the PDOS of the central atom is very close to the case where the CoPc is deposited on Co(111) without the STM tip. Similarly, in the APC (Fig. 6(b)), the spin-up and spin-down states are shifted negatively, and these shifts depend on the tipCoPc distance. However, it is important to point out that these states are not shifted in

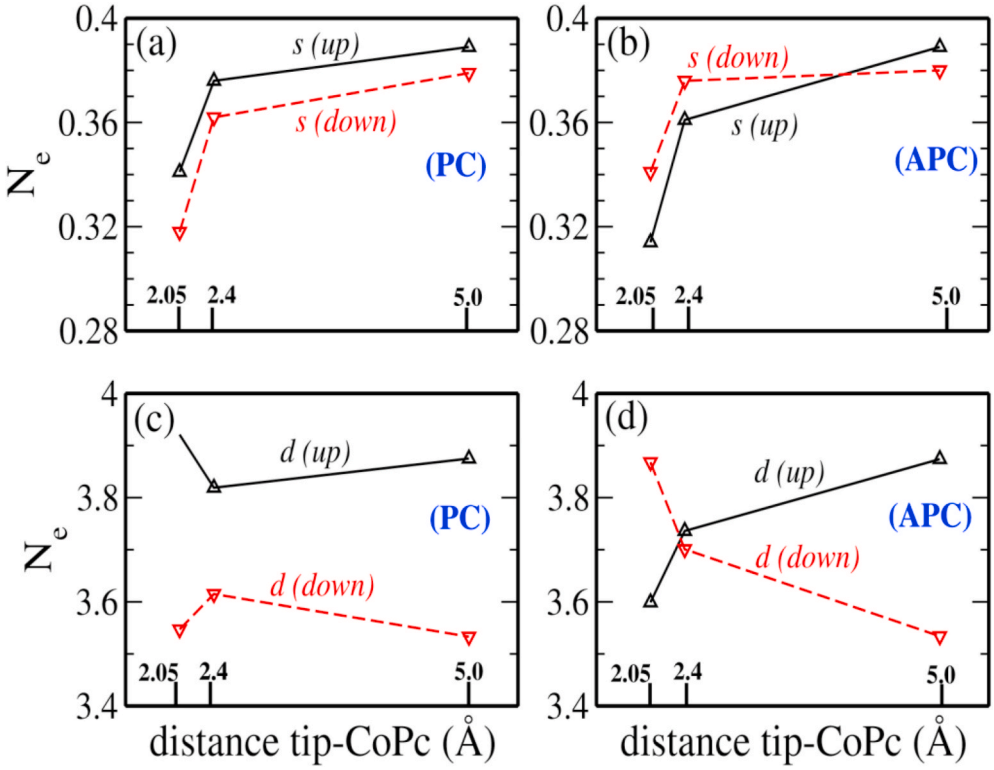

Fig. 5. Spin polarized electron distributions in the *s* and *d* orbitals of Co in CoPc as a function of the tip-CoPc distance in (a) (c) the parallel configuration (PC) and (b) (d) the anti-parallel configuration (APC). Panel (d) shows the crossover of the *d* spin populations as a function of the substrate-tip distance.

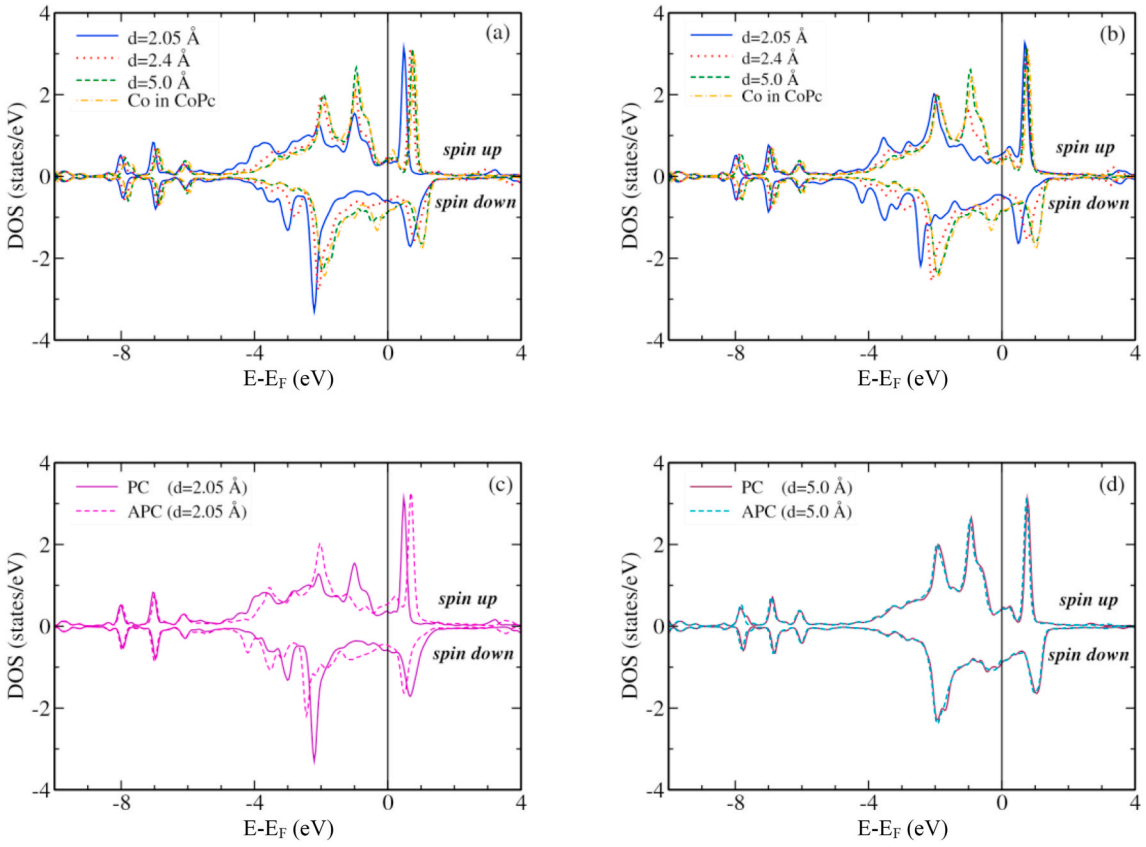

Fig. 6. Density of states of the Co in CoPc in the parallel (a) and anti-parallel (b) configurations for the tip-substrate distance of 2.05 (blue), 2.4 (doted red) and 5.0 Å (dashed green) compared to that of Co in CoPc without tip-molecule interaction (dot-dashed orange). Panels (c) and (d) show the DOS for both configurations (PC and APC) at 2.05 Å and 5 Å respectively. (For interpretation of the references to colour in this figure legend, the reader is referred to the Web version of this article.)

the same way. The shift of the spin-up states is smaller in comparison to that of the spin-down states. This explains the observed transition of the magnetic state from ferromagnetic to antiferromagnetic. Finally, we compare in Fig. 6(c) and (d) the PDOS of the central atom determined in both configurations (PC and APC) in the contact (d = 2.05 Å) and the tunneling (d = 5.0 Å) regimes. In the contact regime (Fig. 6(c)), the spin-up and spin-down states have population inversion, which implies a positive (negative) magnetic moment in the PC (APC). In the tunneling regime (Fig. 6(d)), the difference between the PC and APC DOS is almost negligible, and the spin-up states are dominant, implying a positive magnetic moment for both configurations.

3.3. Transport properties

The main conclusion of the previous section is that the interaction between the Co-tip and CoPc molecule plays an important role in the modification of the magnetic moments of the central atom in CoPc. At this stage, one wonders what is the possible influence of this interaction on the transport properties. To find out, we have first performed electronic transport calculations at zero bias. Fig. 7 shows the transmission coefficients calculated in the tunneling regime (d = 5.0 Å), the Co spin transition regime (d = 2.4 Å) and the contact regime (d = 2.05 Å) for both the PC and the APC. In the tunneling regime (d = 5 Å) where the tip-molecule interaction is weak, we observe that the transmission coefficients are very small for the PC and the APC. At d = 2.05 Å and d = 2.4 Å for the PC (Fig. 7(a)), the transmission at the Fermi level of the spin-up is almost the same in all ranges, and the transmission of the spin down increases when the tip-CoPc separation decreases. However, in the APC we observe a different behavior (see Fig. 7(b)). The transmission of the spin up increases. We deduce that the increase of the separation of the tip and the molecule leads to a reduction of the transmission in the two configurations. This indicates that the electron transfer rate between the tip and CoPc in the contact regime is much larger than that in the in the tunneling regime. In order to describe the effect of the interaction between the tip and CoPc on the electronic transport at zero bias, we show in Fig. 8 the variation of the conductance when the Co tip approaches the central Co atom of the CoPc, for both the PC (Fig. 8-(a)) and the APC (Fig. 8-(b)). At zero bias the conductance, G, is simply $G = (e^2/h)T\,(E_F)$, where e is the electron charge, h the Planck's constant, and $T\,(E_F)$ is the transmission coefficient calculated at E_F.

In the PC, the conductance of the spin-down states (Fig. 8(a)) is larger than that of the spin-up states in the contact regime whereas they are very close in the tunneling regime. In the APC, the conductance of spin-up states (Fig. 8(b)) dominates in the contact regime, and above 2.4 Å, the conductance of spin-down states starts dominating because the magnetic moment of Co in CoPc changed sign and started increasing. Such an explanation can be drawn from the analysis of the orbital projected density of states PDOS of the tip atom and the central atom in CoPc. As the main contribution is obviously from the d states, we show in Figs. 9 and 10 the PDOS of 3d orbitals of the Co-tip and the Co atom of CoPc, respectively. For the Co-tip atom, Fig. 9 shows that the spin-down (spin-up) states dominate at the vicinity of the Fermi level in the PC (APC). As for the central atom of CoPc, Fig. 10 shows that the number of majority and minority states at the Fermi level depend strongly on the tip-CoPc distance. In addition, this figure shows that the main contribution to the PDOS of the majority and minority states is from d_{xz}, d_{yz} and d_z^2, which participate the most to the transmission.

In the PC (Fig. 10, left), our calculation shows that the contribution of the spin-down states at the Fermi level dominates over the whole interval for the Co atom of CoPc. This explains why the conductance of the spin-down states is the most important (see Fig. 8(a)). However, for the APC (Fig. 10 right), the spin-up states dominate at the Fermi level in the contact regime and the spin-down states dominate in the tunneling regime. This explains qualitatively why the total APC conductance is dominated by the spin-up (down) states in the contact (tunneling) regime, respectively. We note that this transition starts from the tip-CoPc distance of 2.4 Å where the contributions of the spin-up and spin-down states are nearly same. In fact, this transition is due to the hybridization strength of the tip and CoPc molecule. We can also remark that in the tunneling regime (d = 5.0 Å) the Co in CoPc DOS at the Fermi level for both configurations are same. This explains why in the tunneling regime the difference between the PC and APC conductances is very small.

We note that for the contact regime the total PC conductance is larger than that of the APC. This last result can be explained by the number of states available at the Fermi level. In the PC, the spin polarized current should be larger and dominated by spin down current, as the tip and the Co(111) substrate have essentially spin down states at the Fermi level (see Figs. 3 and 9). In the APC, the Co of CoPc flips its spin and therefore the DOS at the Fermi level of the tip is dominated by the spin up states. This will result in a smaller current because the Co(111) DOS is still dominated by the spin-down states at the Fermi level.

At 2.4 Å (spin transition regime) the parallel and antiparallel configurations have almost identical conductances. On the other hand, the total conductance in the tunneling regime is always lower than that of the APC. Finally, we note that the total conductance, in both configurations, decreases exponentially when the tip-CoPc distance increases.

We can now calculate the (*Magneto-Resistance*) ratio (MR) as a function of the tip-CoPc separation (d) at zero bias, as $MR(d) = (G^{APC}(d) - G^{PC}(d))/G^{PC}(d)$. Fig. 11 shows the calculated values for the MR. In fact, the changes in the conductances lead to very different values for the MR. In the contact (tunneling) regime, we have a negative (positive) MR, where the total conductance $G^{PC}(G^{APC})$ is larger than the $G^{APC}(G^{PC})$. At the transition point the MR is approximately zero, this is verified by the very small difference between the total G^{PC} and G^{APC} conductances (see Fig. 8). In the tunneling regime, at 3.0 Å (and at 6.0 Å) our calculated value 34.82% (43.63%) could be compared to future experimental results. Iacovita and coworkers [11] have measured the differential

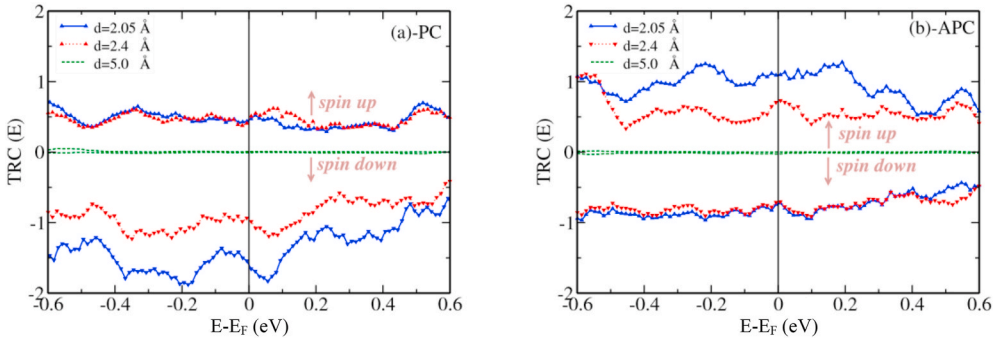

Fig. 7. Zero bias transmission coefficients for different tip-CoPc distance separations d = 2.05 Å (blue triangles), d = 2.4 Å(red triangles), d = 5.0 Å (dashed green), (a) for parallel configuration and (b) for anti-parallel configuration. Spin up are shown above zero, and spin down below zero for clarity only. (For interpretation of the references to colour in this figure legend, the reader is referred to the Web version of this article.)

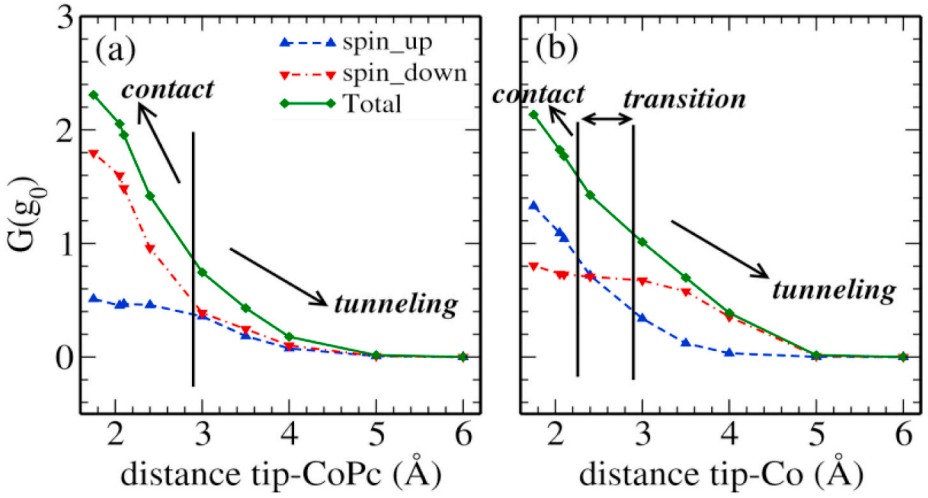

Fig. 8. Total, spin-up (blue triangles) and spin-down (red triangles) conductances at the Fermi level in units of $g_0 = 2e^2/h$, as a function of the tip-CoPc distance in the (a) parallel and (b) anti-parallel configurations. (For interpretation of the references to colour in this figure legend, the reader is referred to the Web version of this article.)

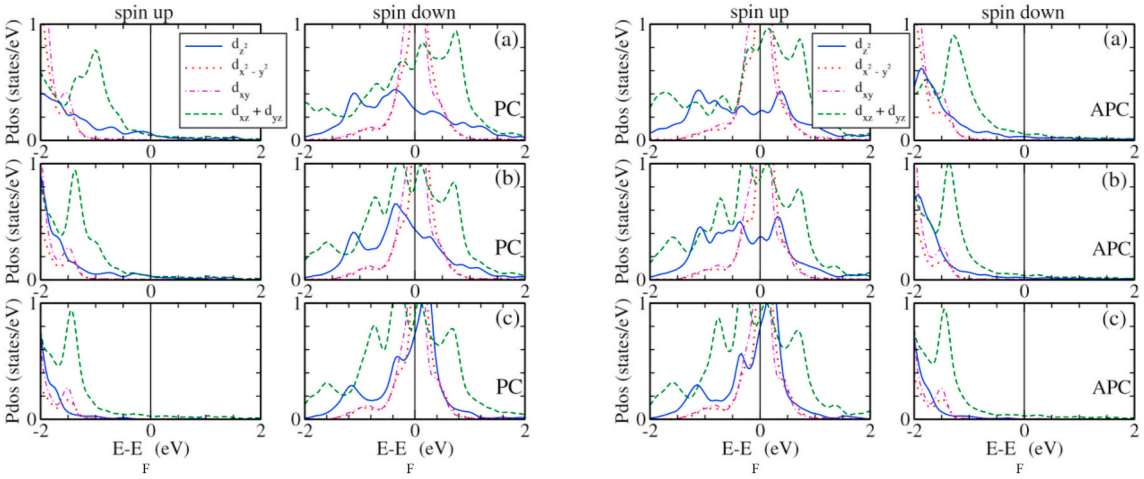

Fig. 9. Spin-polarized projected density of states of the tip atom in the parallel (left) and anti-parallel (right) configurations. (a), (b) and (c) represent the PDOS at 2.05, 2.4 and 5.0 Å, respectively.

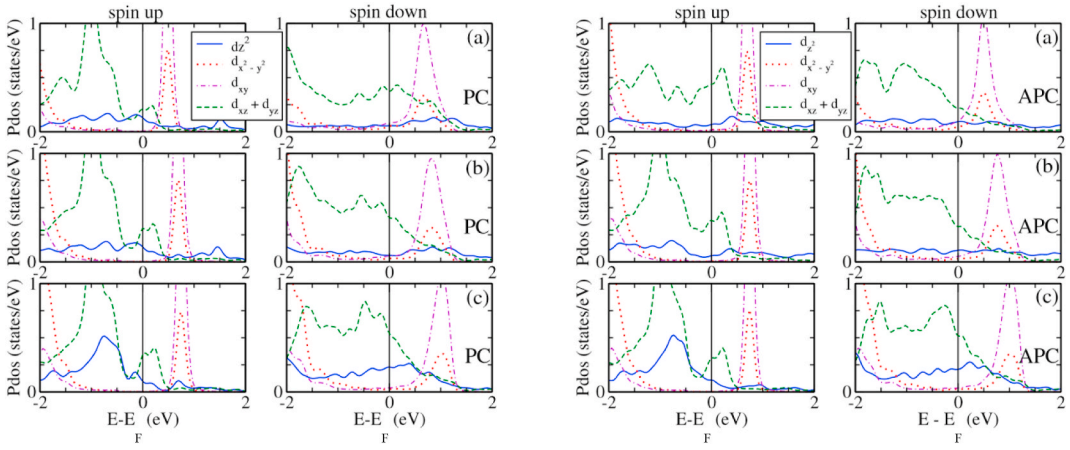

Fig. 10. Spin projected density of states of Co in CoPc in the parallel (left) and anti-parallel (right) configurations. (a), (b) and (c) represent the PDOS at 2.05, 2.4 and 5.0 Å, respectively.

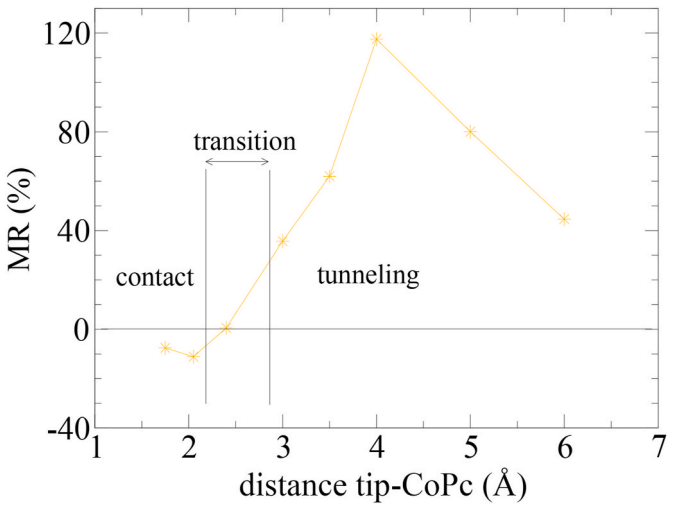

Fig. 11. Calculated magneto-resistance (MR) as a function of the tip-CoPc separation at zero bias.

conductance of CoPc adsorbed on Co(111) islands but it is difficult to compare our results with theirs as they found that their values of the MR are very dependent on the type of the tip. Also it is not known how the CoPc molecule is coupled to the substrate, as the PC and APC conductances are measured on different Co(111) nanoislands of opposite magnetizations grown on Cu(111).

3.4. Bias-dependent I–V characteristics

In this subsection we will analyze the I–V characteristics. The total tunneling current calculated for both configurations where the spin orientation of the magnetic tip is aligned either parallel (PC) or anti-parallel (APC) to that of the magnetic substrate is shown in Fig. 12 for the contact (Fig. 12-(a)) and tunneling (Fig. 12-(b)) regimes. The contributions of the total current of spin-up and spin-down electrons in both PC and APC are also shown. In the contact regime the spin-up and spin-down currents in the two configurations (Fig. 12(a)-PC and Fig. 12(a)-APC) show an ohmic linear dependence over the voltage, and consequently the total current shows the same feature. Unlike the contact regime, in the tunneling regime and in both configurations (Fig. 12(b)-PC and Fig. 12(b)-APC), the spin polarized currents and the total current present non-ohmic behavior. In addition, in the tunneling regime, the most remarkable result is that the spin-up and spin-down currents are almost same in the PC. However for the APC, the spin-up current slightly decreases in contrast to an increase of spin-down current. In addition, the total current obtained in the APC is larger than that in the PC. As for the contact regime, we observe almost equal spin-up and spin-down currents in the APC (Fig. 12(a)-APC), in contrast to the behavior in the tunneling regime (Fig. 12(b)-APC). However, in the APC of the contact regime, we can distinguish that the spin-up current is larger than the spin-down current (Fig. 12(a)-APC), which is different than that observed in the tunneling regime (Fig. 12(b)-APC). The total current for the PC (Fig. 12(a)-PC) and APC (Fig. 12(a)-APC) are almost identical in the contact regime. In the case where a positive (negative) bias voltage is applied to the left electrode, the electrochemical potential of the right electrode is shifted up (down) [45,46], and hence the density of states at the right molecule-substrate will be shifted up (down). Since the transmission coefficient is linked to the density of states at the right molecule-electrode interface, the evolution of the transmission spectra will be mainly determined by the shift of the electrochemical potential in the right electrode. In order to analyze our results of *I–V* curves, we discuss the transmission spectra calculated at zero bias around Fermi level, precisely between −200 meV and +200 meV.

Fig. 13 (which is a blow up and rearrangement of Fig. 7 from −0.3 to +0.3 eV) shows the spin-polarized transmission spectra for the contact and tunneling regimes. In the PC, we can observe that the difference between the majority and the minority spin transmissions is very small in the tunneling regime (Fig. 13(b)). However, in the contact regime this difference is more pronounced, i.e., the spin-down transmission is much larger than the spin-up transmission all over the interval [-0.2,+0.2] (eV). These two remarks explain the small and large difference which was observed between the spin-up and spin-down currents in the tunneling (Fig. 12(b)-PC) and contact regime, respectively (Fig. 12(a)-PC). On the other hand, the transmission coefficient for the APC, shows

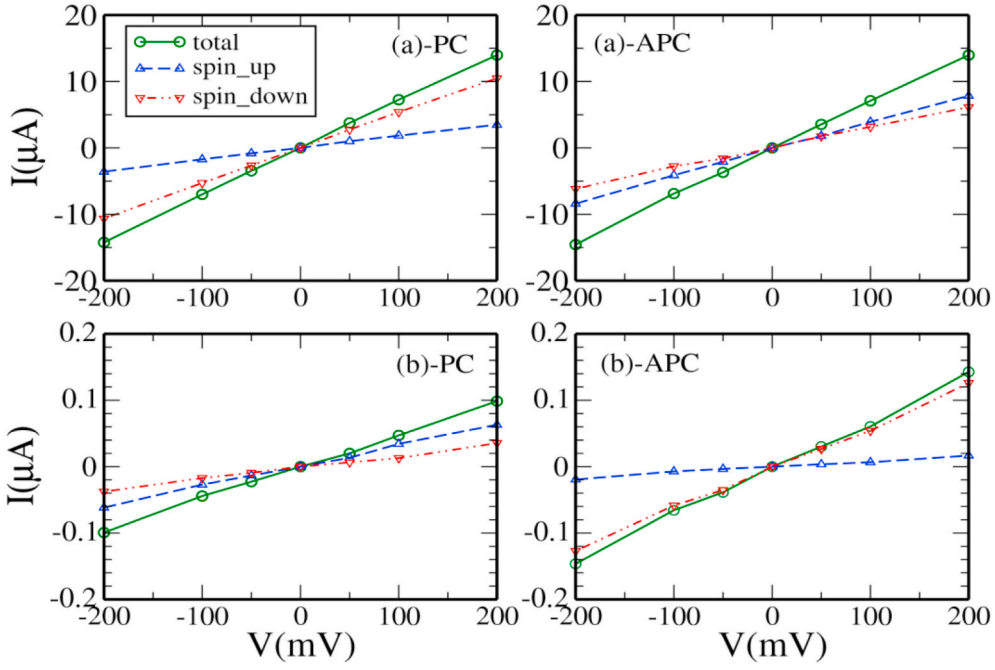

Fig. 12. Spin-polarized current *I* as function of voltage *V* for both PC and APC in the contact (a) and the tunneling (b) regimes. The tip-CoPc separation is 2.05 Å (5.0 Å) in the contact (tunneling) regime.

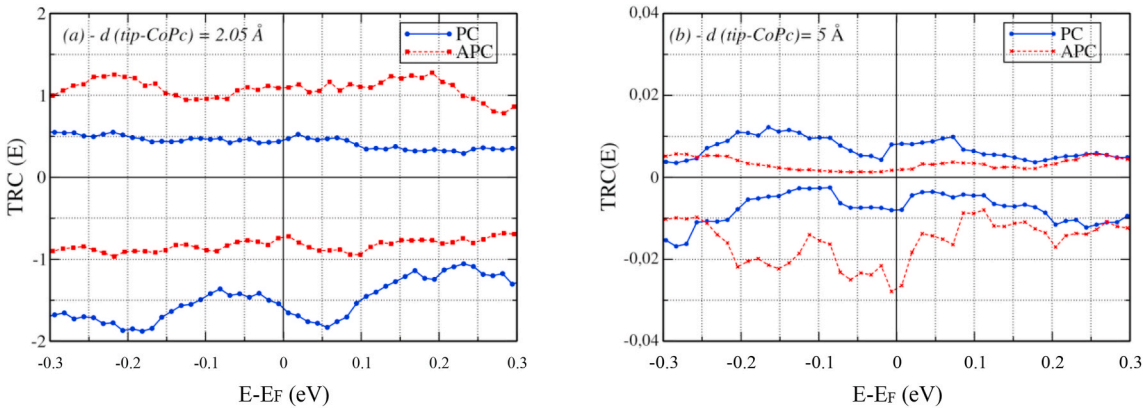

Fig. 13. Zero bias transmission coefficient for parallel and antiparallel configurations in contact (at distance 2.05 Å) and tunneling (at distance 5 Å) regimes. Spin-up transmissions are represented above zero and spin-down transmissions below zero for clarity only.

that the spin-down transmission becomes larger than that of spin-up in the tunneling regime (Fig. 13(b)). We can also observe that the spin-up and spin-down transmissions become almost equal in the contact regime (Fig. 13(a)). The two observations explain why the total current in the tunneling regime is dominated by the *spin-down* current (Fig. 12(b)-APC), and that the spin-up and spin-down spin currents are almost equal in the contact regime (Fig. 12(a)-APC).

4. Conclusion

In this work, we have shown the impact of a Co(111) magnetic substrate and Co STM tip on the physical properties of CoPc molecule using density functional theory in conjunction with Non-Equilibrium Green's function transport method using the Landauer formula. We have shown that the spin magnetic moment of CoPc molecule can be flipped by varying the distance between the STM tip and the CoPc molecule when passing from the tunneling regime to the contact regime. Our calculations show that this spin flip of CoPc molecule led to a change of the sign of the *Tunneling Magneto-Resistance* ratio (TMR). The change from the tunneling regime to the contact regime also produced large modifications of the total and spin-polarized *I–V* characteristics.

CRediT authorship contribution statement

A. Jaafar: Formal analysis, made the calculations, analyzed the results. **I. Rungger:** provided the Smeagol electronic transport software. **S. Sanvito:** the Smeagol electronic transport software. **M. Alouani:** Formal analysis, Supervision, conceived the project and supervised the calculations, analyzed the results, wrote the manuscript with input from all authors.

Declaration of competing interest

The authors declare that they have no known competing financial interests or personal relationships that could have appeared to influence the work reported in this paper.

Acknowledgments

This work of the Interdisciplinary Thematic Institute QMat, as part of the ITI 2021 2028 program of the University of Strasbourg, CNRS and Inserm, was supported by IdEx Unistra (ANR 10 IDEX 0002), and by SFRI STRATUS project (ANR 20 SFRI 0012) and EUR QMAT ANR-17-EURE-0024 under the framework of the French Investments for the Future Program. This work was performed using HPC resources from GENCI-CINES Grant gem1100 and the HPC supercomputer of the University of Strasbourg.

References

[1] M.A. Reed, T. Lee, Molecular Nanoelectronics, American Scientific Publishers, Stevenson Ranch, CA, 2003.
[2] L.G.G.V. Dias da Silva, M.L. Tiago, S.E.L. Ulloa, F. Reboredo, E. Dagotto, Many-body electronic structure and Kondo properties of cobalt-porphyrin molecules, Physiol. Physicians B 80 (2009) 155443.
[3] L. Vitali, et al., Phys. Rev. Lett. 101 (2008) 216802.
[4] A. Scheybal, T. Ramsvik, R. Bertschinger, M. Putero, F. Nolting, T.A. Jung, Induced magnetic ordering in a molecular monolayer, Chem. Phys. Lett. 411 (2005) 214.
[5] H. Wende, M. Bernien, J. Luo, C. Sorg, N. Ponpandian, J. Kurde, J. Miguel, M. Piantek, X. Xu, Ph. Eckhold, Nat. Mater. 6 (2007) 516520.
[6] Z.T. Liu, H.S. Kwok, A.B. Djurisic, The optical functions of metal phthalocyanines, J. Phys. D Appl. Phys. 37 (2004) 678.
[7] J.A.A.W. Elemans, R. van Hameren, R.J.M. Nolte, A.E. Rowan, Molecular Materials by self-assembly of porphyrins, phthalocyanines, and perylenes, Adv. Mater. 18 (2006) 1251.
[8] A. Zhao, Q. Li, L. Chen, H. Xiang, W. Wang, S. Pan, B. Wang, X. Xiao, J. Yang, J. G. Hou, Q. Zhu, Science 309 (2005) 1542.
[9] G. Chiappe, E. Louis, Phys. Rev. Lett. 97 (2006), 076806.
[10] J.M. Aguiar-Hualde, G. Chiappe, E. Louis, E.V. Anda, Phys. Rev. B 76 (2007) 155427.
[11] C. Iacovita, M.V. Rastei, B.W. Heinrich, T. Brumme, J. Kortus, L. Limot, J. P. Bucher, Phys. Rev. Lett. 101 (2008) 116602.
[12] A.F. Takács, F. Witt, S. Schmaus, T. Balashov, M. Bowen, E. Beaurepaire, W. Wulfhekel, Phys. Rev. B 78 (2008) 233404.
[13] L. Chen, Z. Hu, A. Zhao, B. Wang, Y. Luo, J. Yang, J.G. Hou, Phys. Rev. Lett. 99 (2007) 146803.
[14] A. Calzolari, A. Ferretti, M.B. Nardelli, Nanotechnology 18 (2007) 424013.
[15] X. Chen, Y. Fu, S. Ji, T. Zhang, P. Cheng, X. Ma, X. Zou, W. Duan, J. Jia, Q. Xue, Phys. Rev. Lett. 101 (2008) 197208.
[16] L. Gao, W. Ji, Y.B. Hu, Z.H. Cheng, Z.T. Deng, Q. Liu, N. Jiang, X. Lin, W. Guo, S. X. Du, W.A. Hofer, X.C. Xie, H.-J. Gao, Phys. Rev. Lett. 99 (2007) 106402.
[17] Xi Chen, M. Alouani, Phys. Rev. B 82 (2010), 094443.
[18] S. Javaid, M. Bowen, S. Boukari, L. Joly, J.-B. Beaufrand, Xi Chen, Y.J. Dappe, F. Scheurer, J.-P. Kappler, J. Arabski, W. Wulfhekel, M. Alouani, E. Beaurepaire, Phys. Rev. Lett. 105 (2010), 077201.
[19] C. LeGall, et al., Phys. Rev. Lett. 102 (2009) 127402.
[20] M. Goryca, et al., Phys. Rev. Lett. 103 (2009), 087401.
[21] K. von Bergmann, et al., Phys. Rev. Lett. 96 (2006) 167203.
[22] C.F. Hirjibehedin, et al., Science 312 (2006) 1021.
[23] P. Wahl, et al., Phys. Rev. Lett. 98 (2007), 056601.
[24] C.F. Hirjibehedin, et al., Science 317 (2007) 1199.
[25] B.W. Heinrich, et al., Phys. Rev. B 79 (2009) 113401.
[26] Y. Yayon, et al., Phys. Rev. Lett. 99 (2007), 067202.
[27] W.A. Hofer, et al., Rev. Mod. Phys. 75 (2003) 1287.
[28] N. Néel, J. Kröger, R. Berndt, Phys. Rev. B 82 (2010) 233401.
[29] R.Z. Huang, V.S. Stepanyuk, A.L. Klavsyuk, W. Hergert, P. Bruno, J. Kirschner, Phys. Rev. B 73 (2006) 153404.
[30] N. Néel, J. Kröger, L. Limot, K. Palotas, W.A. Hofer, R. Berndt, Phys. Rev. Lett. 98 (2007), 016801.
[31] Kun Tao, V.S. Stepanyuk, W. Hergert, I. Rungger, S. Sanvito, P. Bruno, Phys. Rev. Lett. 103 (2009), 057202.
[32] J.M. Soler, E. artacho, J.D. Gale, A. Garcia, J. Junquera, P. Ordejon, D. sanchez-Portal, J. Phys. Condens. Matter 14 (2002) 2745.
[33] http://www.smeagol.tcd.ie.
[34] A.R. Rocha, Nat. Mater. 4 (2005) 335.
[35] F. Evers, R. Korytár, S. Tewari, J.M. van Ruitenbeek, Rev. Mod. Phys. 92 (2020), 035001.
[36] N. Troullier, J.L. Martins, Phys. Rev. B 43 (1991) 1993.

[37] M. Payne, M. Teter, D. Allan, T. Arias, J.D. Joannopoulos, Rev. Mod. Phys. 64 (1992).
[38] J.P. Perdew, K. Burke, M. Ernzerhof, Phys. Rev. Lett. 77 (1996) 3865.
[39] Ceperley-Alder, Phys. Rev. B 23 (1981) 5075.
[40] S. Grimme, J. Comput. Chem. 27 (2006) 1787.
[41] L. Kleinmann, D.M. Bylander, Phys. Rev. B 48 (1982) 1425.
[42] H.J. Monkhorst, D.J. Pack, Phys. Rev. B 13 (1976) 5188.
[43] I. Rungger, S. Sanviton, Phys. Rev. B 78 (2008), 035407.
[44] S. Datta, in: H. Ahmed, M. Pepper, A. Broers (Eds.), Electronic Transport in Mesoscopic, Cambridge University Press, Combridge, England, 1995.
[45] S. Datta, Nanotechnology 15 (2004) S433.
[46] S. Datta, Quantum Transport: Atom to Transistor, Cambridge University Press, New York, 2005.
[47] H. Haug, A.P. Jauho, Quantum Kinetics in Transport and Optics of Semiconductors, Springer-Verlag, Berlin, 1996.
[48] C. Toher, A. Filippetti, S. Sanvito, K. Burke, Phys. Rev. Lett. 95 (2005) 146402.
[49] J.B. Neaton, M.S. Hybertsen, S.G. Louie, Phys. Rev. Lett. 97 (2006) 216405.
[50] J.E. Brumboiu, S. Haldar, J. Lüder, O. Eriksson, H.C. Herper, B. Brena, B. Sanyal, J. Chem. Theor. Comput. 12 (2016) 1772.
[51] R.Z. Huang, et al., Phys. Rev. B 73 (2006) 153404.